

Structural and dynamical properties of superfluid helium: A density-functional approach

F. Dalfovo and A. Lastri

Dipartimento di Fisica, Università di Trento, 38050 Povo, Italy

L. Pricaupenko

Division de Physique Théorique, Institute de Physique Nucléaire, 91406 Orsay Cedex, France

S. Stringari

Dipartimento di Fisica, Università di Trento, 38050 Povo, Italy

J. Treiner

Division de Physique Théorique, Institute de Physique Nucléaire, 91406 Orsay Cedex, France

(Received 15 December 1994)

We present a density functional for liquid ^4He , properly accounting for the static response function and the phonon-roton dispersion in the uniform liquid. The functional is used to study both structural and dynamical properties of superfluid helium in various geometries. The equilibrium properties of the free surface, droplets, and films at zero temperature are calculated. Our predictions agree closely with the results of *ab initio* Monte Carlo calculations, when available. The introduction of a phenomenological velocity-dependent interaction, which accounts for backflow effects, is discussed. The spectrum of the elementary excitations of the free surface and films is studied.

I. INTRODUCTION

The aim of the present work is to present a density-functional theory, which treats static and dynamic properties of liquid helium on the same ground and is accurate at the microscopic level.

The investigation of the properties of liquid helium in different geometries has a long story. Extensive work has been devoted to the search for and the understanding of superfluid effects in finite systems like helium droplets or in quasi-two-dimensional systems like helium films on solid substrates or within porous materials. Liquid helium exhibits very peculiar properties, such as the propagation of surface modes in the short-wavelength regime, quantum evaporation of atoms produced by rotons impinging on the surface, and wetting and prewetting transitions on solid substrates. The nucleation of bubbles at negative pressure and the nucleation of quantized vortices near walls are further examples of interesting phenomena where both the inhomogeneity of the liquid and quantum correlations play an important role. These phenomena, among others, make liquid helium particularly appealing from the viewpoint of quantum many-body theories. Theory and experiments, however, have not yet a satisfactory overlap. One difficulty comes from the fact that *ab initio* calculations are still hard to implement for inhomogeneous systems. On the other hand, phenomenological theories, which are quite successful in describing macroscopic properties, are not always adequate enough to investigate the behavior of the system on the scale of interatomic distances. A major progress in this direc-

tion has been recently made in the framework of density-functional theory (DFT).

Several density functionals have been developed in the last years for applications to quantum fluids. The method consists of writing the energy of the many-body system as a functional of the one-body density; from a given functional one extracts the equilibrium state, by minimizing the energy with respect to the density, as well as the excited states, by solving time-dependent equations of motion. An accurate phenomenological density-functional for liquid ^4He (Orsay-Paris functional) has been recently introduced;¹ it has proved to be quite reliable in different contexts, such as helium films and wetting phenomena,²⁻⁶ vortices in bulk liquid,⁷ or droplets.⁸ For dynamical properties it gives predictions which are close to the Feynman approximation for elementary excitations. In particular it does not account for backflow effects.⁹

In the present work we present a new functional. We follow the same ideas which lead to the Orsay-Paris functional, taking a similar two-body interaction of the Lennard-Jones type and including phenomenologically short-range correlations. The main difference with respect to the Orsay-Paris functional is the addition of two new terms which allow for a better description of both static and dynamic properties on the scale of the interatomic spacing. These terms are (i) a nonlocal term depending on gradients of the density, which allows one to reproduce the experimental static response function in a wide range of wave vectors, as well as its pressure dependence, and (ii) a term depending on local variations of

the velocity field (backflow effects), which allows one to reproduce the experimental phonon-roton dispersion in bulk.

The velocity-dependent term has a form similar to the one already introduced by Thouless,¹⁰ who studied the flow of a dense superfluid. The idea is to model backflow effects, which are important at small wavelengths, by a nonlocal kinetic energy term.

With these ingredients the predictions for several properties of nonuniform systems are significantly improved with respect to the ones given by previous functionals. The accuracy of the density functional theory is now comparable to the one of *ab initio* Monte Carlo calculations. The resulting approach, although phenomenological, represents a powerful and accurate tool whenever *ab initio* calculations become hard to implement. It allows one to investigate a wide variety of systems of different sizes and in different geometries, from few atoms to the bulk liquid, with limited numerical efforts.

The paper is organized as follows: in Sec. II we introduce the density functional for static calculations. We emphasize and motivate the differences with respect to the Orsay-Paris functional. The results for the equilibrium properties of the free surface, droplets, and films are given in Sec. III. In Sec. IV we discuss the application of the density-functional theory to dynamics, showing the connection with the Feynman approximation and with the formalism of the random phase approximation. We introduce a phenomenological current-current interaction which makes the density-functional quantitative in the description of the spectrum of excited states. We discuss the role of this new term using sum rule arguments. Finally, in Sec. V we present the results for the excited states of the free surface and of films.

II. GROUND STATE CALCULATIONS

In the density-functional formalism at zero temperature, the energy of a Bose system is assumed to be a functional of a complex function Ψ :

$$E = \int d\mathbf{r} \mathcal{H}[\Psi, \Psi^*] . \quad (1)$$

The function Ψ is written in the form

$$\Psi(\mathbf{r}, t) = \Phi(\mathbf{r}, t) \exp\left(\frac{i}{\hbar} S(\mathbf{r}, t)\right) . \quad (2)$$

The real function Φ is related to the diagonal one-body density by $\rho = \Phi^2$, while the phase S fixes the velocity of the fluid through the relation $\mathbf{v} = (1/m)\nabla S$. In the calculation of the ground state, only states with zero velocity are considered, so that the energy is simply a functional of the one-body density $\rho(\mathbf{r})$. A natural representation is given by

$$E = \int d\mathbf{r} \mathcal{H}_0[\rho] = E_c[\rho] + \int d\mathbf{r} \frac{\hbar^2}{2m} (\nabla\sqrt{\rho})^2, \quad (3)$$

where the second term on the right-hand side (RHS) is

a quantum pressure, corresponding to the kinetic energy of a Bose gas of nonuniform density. The quantity $E_c[\rho]$ is a ‘‘correlation energy’’; it incorporates the effects of dynamic correlations induced by the interaction.

Ground state configurations are obtained by minimizing the energy of the system with respect to the density. This leads to the Hartree-type equation

$$\left\{ -\frac{\hbar^2}{2m} \nabla^2 + U[\rho, \mathbf{r}] \right\} \sqrt{\rho(\mathbf{r})} = \mu \sqrt{\rho(\mathbf{r})} , \quad (4)$$

where $U[\rho, \mathbf{r}] \equiv \delta E_c / \delta \rho(\mathbf{r})$ acts as a mean field, while the chemical potential μ is introduced in order to ensure the proper normalization of the density to a fixed number of particles.

For a weakly interacting Bose system the expression of \mathcal{H}_0 can be derived on a rigorous basis, yielding the well-known Gross-Pitaevskii theory.¹¹ Since liquid helium is a strongly correlated system, such a derivation, starting from first principles, is not available. One then resorts to approximate schemes for the correlation energy. Krotscheck and co-workers,^{12–14} for instance, have developed a variational hypernetted-chain–Euler-Lagrange (HNC-EL) theory in which the one-body effective potential U is evaluated using the microscopic Hamiltonian. An alternative approach consists of writing a phenomenological expression for the correlation energy, whose parameters are fixed to reproduce known properties of the bulk liquid.

A simple functional was introduced in Refs. 15 and 16 to investigate properties of the free surface and droplets of both ⁴He and ³He. The correlation energy, in analogy with the formalism of zero-range Skyrme interactions in nuclei,¹⁷ was written as

$$E_c[\rho] = \int d\mathbf{r} \left[\frac{b}{2} \rho^2 + \frac{c}{2} \rho^{2+\gamma} + d(\nabla\rho)^2 \right] , \quad (5)$$

where b , c , and γ are phenomenological parameters fixed to reproduce the ground state energy, density, and compressibility of the homogeneous liquid at zero pressure, and d is adjusted to the surface tension of the liquid. The first two terms correspond to a local density approximation for the correlation energy, and nonlocal effects are included through the gradient correction. The local density approximation is currently used to describe exchange-correlation energy in electron systems; its use for liquid helium does not provide quantitative results.¹⁸ Nonlocal terms, like $(\nabla\rho)^2$ in (5), turn out to be crucial for the description of inhomogeneous liquid helium. Nonlocality effects have been included in DFT in a more realistic way by Dupont-Roc *et al.*,¹ who generalized Eq. (5) accounting for the finite range of the atom-atom interaction. The resulting functional has proved to be reliable in describing several inhomogeneous systems.^{1–8}

In the present work we follow the spirit of Ref. 1. We use a similar two-body finite-range interaction screened at short distances and a weighted density (or ‘‘coarse-grained’’ density) to account for short-range correlations. The most important feature of this approach is that the

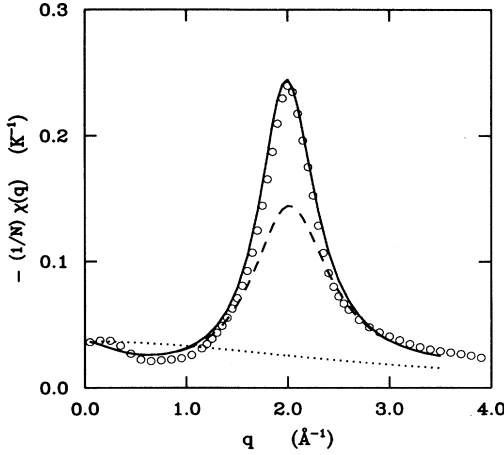


FIG. 1. Static response function in liquid ${}^4\text{He}$ at zero pressure. Points, experimental data (Ref. 20); dotted line, from functional of Refs. 15, 16; dashed line, Orsay-Paris functional (Ref. 1); solid line, present functional [Eq. (11)].

static response function of the liquid can be reproduced even at finite wave vectors q , up to the roton region. The static response function $\chi(q)$ fixes the linear response of the system to static density-perturbations and is a key quantity in density-functional theories. It is easily calculated from functional (3) by taking the second functional derivative of the energy in q space:¹⁹

$$-\chi^{-1}(q) = \frac{\hbar^2 q^2}{4m} + \frac{\rho}{V} \int d\mathbf{r} d\mathbf{r}' \frac{\delta^2 E_c}{\delta\rho(\mathbf{r})\delta\rho(\mathbf{r}')} e^{-i\mathbf{q}\cdot(\mathbf{r}-\mathbf{r}')} . \quad (6)$$

$$\begin{aligned} \mathcal{H}_0 = & \frac{\hbar^2}{2m} (\nabla\sqrt{\rho})^2 + \frac{1}{2} \int d\mathbf{r}' \rho(\mathbf{r}) V_l(|\mathbf{r}-\mathbf{r}'|) \rho(\mathbf{r}') + \frac{c_2}{2} \rho(\mathbf{r}) (\bar{\rho}_r)^2 + \frac{c_3}{3} \rho(\mathbf{r}) (\bar{\rho}_r)^3 \\ & - \frac{\hbar^2}{4m} \alpha_s \int d\mathbf{r}' F(|\mathbf{r}-\mathbf{r}'|) \left(1 - \frac{\tilde{\rho}(\mathbf{r})}{\rho_{0s}}\right) \nabla\rho(\mathbf{r}) \cdot \nabla\rho(\mathbf{r}') \left(1 - \frac{\tilde{\rho}(\mathbf{r}')}{\rho_{0s}}\right) . \end{aligned} \quad (9)$$

The first term on the RHS is the quantum pressure, as in Eq. (3). The second term contains a two-body interaction V_l , which is the Lennard-Jones interatomic potential, with the standard value of the hard core radius of 2.556 Å and of the well depth 10.22 K, screened at short distance ($V_l \equiv 0$ for $r < h$, with $h = 2.1903$ Å). The weighted density $\bar{\rho}$ is the average of $\rho(\mathbf{r})$ over a sphere of radius h :

$$\bar{\rho}(\mathbf{r}) = \int d\mathbf{r} \Pi_h(|\mathbf{r}-\mathbf{r}'|) \rho(\mathbf{r}') , \quad (10)$$

where $\Pi_h(r) = 3(4\pi h^3)^{-1}$ for $r \leq h$ and zero elsewhere. The two terms containing $\bar{\rho}$, with the parameters $c_2 = -2.411857 \times 10^4 \text{ K } \text{Å}^6$ and $c_3 = 1.858496 \times 10^6 \text{ K } \text{Å}^9$, account phenomenologically for short-range correlations. All these terms have a form similar to the Orsay-Paris functional.¹ The Lennard-Jones potential is here screened in a simpler way, avoiding the fourth power

A major advantage of liquid helium is that $\chi(q)$ is known experimentally. It is related to the inverse-energy-weighted moment of the dynamic structure function $S(q, \omega)$, measured in neutron scattering, through the relation

$$\chi(q) = -2m_{-1}(q) , \quad (7)$$

the n moment of $S(q, \omega)$ being defined as

$$m_n(q) = \int_0^\infty d\omega S(q, \omega) (\hbar\omega)^n . \quad (8)$$

The experimental data for $\chi(q)$ in the uniform liquid at zero pressure²⁰ are shown in Fig. 1 (circles). The predictions of the zero-range functional of Ref. 15 [i.e., with the correlation energy given in Eq. (5)] and of the finite-range Orsay-Paris functional¹ are also shown as dotted and dashed lines, respectively. The $q = 0$ limit is fixed by the compressibility of the system, which in both cases is an input of the theory. It ensures the correct behavior in the long-wavelength limit and, consequently, the correct description of systems characterized by smooth density variations as happens, for example, in the free surface or in helium droplets. The height of the peak of the static response function in the roton region, $q \simeq 2 \text{ Å}^{-1}$, is important in characterizing structural properties on the interatomic length scale (for instance, the layered structure of helium films). Therefore, the first important idea is to improve on the Orsay-Paris functional in order to better reproduce the experimental peak of $\chi(q)$ in the roton region.

In the present work, the function \mathcal{H}_0 , entering functional (3), is taken in the form

for $r < h$, and the dependence on $\bar{\rho}$ is slightly different. The effects of these minor changes will be discussed later. The last term in Eq. (9) is a completely new term; it depends on the gradient of the density at different points and corresponds to a nonlocal correction to the kinetic energy. The function F is a simple Gaussian $F(r) = \pi^{-3/2} \ell^{-3} \exp(-r^2/\ell^2)$ with $\ell = 1 \text{ Å}$, while $\alpha_s = 54.31 \text{ Å}^3$. The parameters are fixed to reproduce the peak of the static response function in the bulk liquid. The latter can be easily calculated by using Eq. (6). One finds

$$\begin{aligned} -\chi^{-1}(q) = & \frac{\hbar^2 q^2}{4m} + \rho \hat{V}_l(q) + c_2 [2\hat{\Pi}_h(q) + \hat{\Pi}_h^2(q)] \rho^2 \\ & + 2c_3 [\hat{\Pi}_h(q) + \hat{\Pi}_h^2(q)] \rho^3 \\ & - \frac{\hbar^2}{2m} \alpha_s \rho \left(1 - \frac{\rho}{\rho_{0s}}\right)^2 q^2 \exp\left(-\frac{q^2 \ell^2}{4}\right) , \end{aligned} \quad (11)$$

where $\hat{V}_i(q)$ and $\hat{\Pi}_h(q)$ are the Fourier transforms of the screened Lennard-Jones potential and the weighting function Π_h , respectively, while ρ is the bulk density ($\rho = \rho_0 = 0.021836 \text{ \AA}^{-3}$) is shown in Fig. 1 (solid line). The factor $(1 - \tilde{\rho}/\rho_{0s})$, with $\rho_{0s} = 0.04 \text{ \AA}^{-3}$, is included in order to obtain a pressure dependence of the static response function close to the one predicted by diffusion Monte Carlo simulations.²¹ For instance in the liquid near solidification ($\rho = 0.02622 \text{ \AA}^{-3}$) one finds a peak of $\chi(q)$ about 10% higher than at zero pressure, and displaced by 0.1 \AA^{-1} to larger wavelengths. Finally, the quantity $\tilde{\rho}(\mathbf{r})$ is again a weighted density, calculated using the gradient-gradient interaction function F as a weighting function:

$$\tilde{\rho}(\mathbf{r}) = \int d\mathbf{r}' F(|\mathbf{r} - \mathbf{r}'|) \rho(\mathbf{r}') \quad (12)$$

Actually the density $\tilde{\rho}(\mathbf{r})$ is very close to the particle density $\rho(\mathbf{r})$ except in strongly inhomogeneous situations (like helium adsorbed on a graphite substrate). For this reason one can safely replace $\tilde{\rho}(\mathbf{r})$ with $\rho(\mathbf{r})$ for the investigation of the free surface, helium droplets, and films on weak binding substrates. Stronger constraints on the form of F should be provided by the study of the liquid-solid phase transition.

In a uniform liquid of constant density the energy per particle, from functional (3)(9), reduces to the power law

$$\frac{E}{N} = \frac{b}{2}\rho + \frac{c_2}{2}\rho^2 + \frac{c_3}{3}\rho^3 \quad (13)$$

where $b = -718.99 \text{ K \AA}^3$ is the integral of the screened Lennard-Jones potential V_i . Pressure and compressibility can be derived directly by taking the first and second derivative of the energy:

$$P = \rho^2 \frac{\partial E}{\partial \rho N} \quad , \quad -\chi^{-1}(0) = \frac{\partial P}{\partial \rho} \quad (14)$$

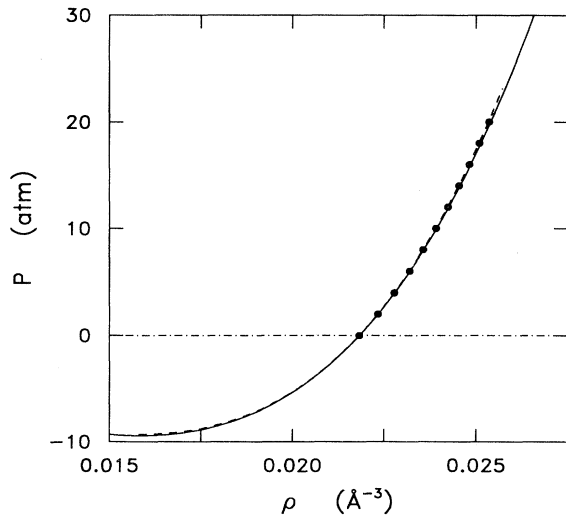


FIG. 2. Pressure versus density in bulk. Points, experimental data (Ref. 24); dashed line, quantum Monte Carlo results (Ref. 22); solid line, present density functional.

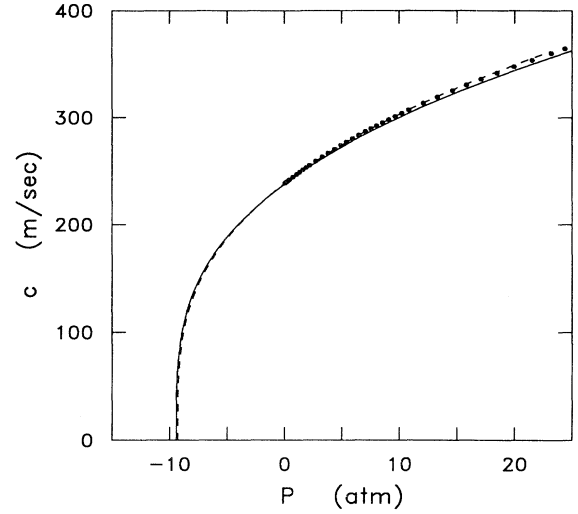


FIG. 3. Sound velocity in bulk. Points, experimental data (Refs. 23); dashed line, quantum Monte Carlo results (Ref. 22); solid line, present density functional.

The experimental values of the density, energy per particle, and compressibility of the uniform system at zero pressure are used as input to fix the parameters h , c_2 , and c_3 . The resulting equation of state and the sound velocity, $c^2 = -[m\chi(0)]^{-1}$, are shown in Figs. 2 and 3, respectively. The comparison with the results of Monte Carlo simulations²² and with experimental data^{23,24} shows that the present density-functional theory describes correctly the ground state of the bulk liquid ^4He at all pressures. Comments about the equation of state in the limit of a quasi-two-dimensional (quasi-2D) liquid will be given when discussing the structural properties of films.

To conclude this section we emphasize again the main idea. The density functional (3),(9) incorporates the correct long-range behavior of the interatomic potential, and accounts for short-range correlations in a phenomenological way. The ground state of the uniform liquid is well reproduced at all pressures and, furthermore, the response to small static density perturbations, up to the roton wavelength, is also correctly reproduced. Significant differences with respect to previous functionals are expected in the predictions of properties which depend on the behavior of the fluid on the interatomic length scale. Some interesting examples are discussed in the following section.

III. RESULTS FOR THE EQUILIBRIUM CONFIGURATION OF FREE SURFACE, DROPLETS, AND FILMS

A. Free surface

To compute the density profile and the energy of a planar free surface of ^4He at zero temperature one has to solve the integro-differential Hartree equation (4) with the mean field U extracted from (9). Both ρ and U

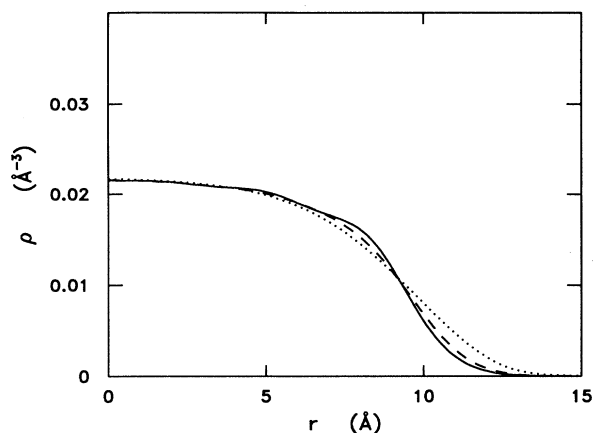


FIG. 4. Free surface profile of liquid ${}^4\text{He}$ at zero temperature. Dotted line, functional of Refs. 15, 16; dashed line, Orsay-Paris functional (Ref. 1); solid line, present functional.

depend only on the coordinate orthogonal to the surface, so that the equation is one dimensional. The integrals on parallel coordinates in the nonlocal terms of the functional can be written analytically. The numerical solution of the nonlinear equation (4) is obtained by means of an iterative procedure and provides the density $\rho(z)$, from which the surface tension σ can be calculated through

$$\sigma = \int dz \{ \mathcal{H}_0[\rho] - \mu\rho \} \quad (15)$$

The bulk density is kept fixed to the experimental value at zero pressure, $\rho_0 = 0.021836 \text{ \AA}^{-3}$. The density profile is shown in Fig. 4, together with the results given by the Skyrme functional of Eq. (5) and the Orsay-Paris one. The surface tension is practically the same in the three cases. The present functional gives $\sigma = 0.272 \text{ K \AA}^{-2}$, to be compared with the experimental values quoted in the literature: 0.275 K \AA^{-2} (Ref. 25) and 0.257 K \AA^{-2} (Ref. 26). The 10%-90% surface thickness is approximately 6 \AA . The value 7.6 \AA , extracted from x-ray scattering data,²⁷ is slightly larger, being closer to the result of the zero-range functional of Eq. (5). However, the experimental value is expected to depend on the form of the density profile used to fit the measured reflectivity.

Notice that the density $\rho(z)$ resulting from expression (9) is not as smooth as the ones given by previous calculations. It exhibits small oscillations which appear as shoulders on the surface profile and asymptotically die in the bulk region. Oscillations of this type were predicted long time ago by Regge.²⁸ In his theory the surface was treated as a source of elementary excitations producing static ripples on the density profile. The form of the ripples was connected to the behavior of the static response function and the pronounced peak at the roton wavelength was associated with the tendency of atoms to localize in "soft sphere close packing." This tendency is opposed by the zero-point motion of the surface, whose thickness is larger than the interparticle distance, and

by compressibility effects, so that the density oscillations turn out to be quite small. The role of the static response function in characterizing the form of the surface profile is clearly seen in Figs. 1 and 4. Of course one expects that functionals describing the short-wavelength behavior of $\chi(q)$ in a correct way will give rise to more reliable predictions for the properties of the fluid in the microscopic scale. It is worth noticing that similar oscillations of the surface profile have been recently predicted in classical fluids interacting through short-ranged potentials.²⁹ In that case, the presence of oscillations is related to the behavior of the radial distribution function by means of the Ornstein-Zernike equation. The connection with our density-functional approach, applied to a quantum fluid interacting through a potential of the Lennard-Jones type, could help to clarify the physical basis of the soft sphere close packing model suggested by Regge.

B. Droplets

The solution of the Hartree equation (4) in spherical symmetry with a fixed number of particles N provides the ground state of ${}^4\text{He}$ droplets. Since the density-functional approach is not time consuming, it allows one to compute the energy and the density profiles of droplets in a wide range of sizes. The density $\rho(r)$ for droplets with $8 \leq N \leq 60$ is shown in Fig. 5. Again one finds ripples on the surface profile; they are more pronounced than in the case of the free surface, since the droplets have a size of the order of a few interatomic distances and the soft sphere close packing tends to produce shell structures. This effect was already suggested by Rasetti and Regge,³⁰ but subsequent theoretical calculations^{16,31-33} did not predict any clear and systematic oscillation in $\rho(r)$. Only recently, sizable oscillations were found in diffusion Monte Carlo (DMC)

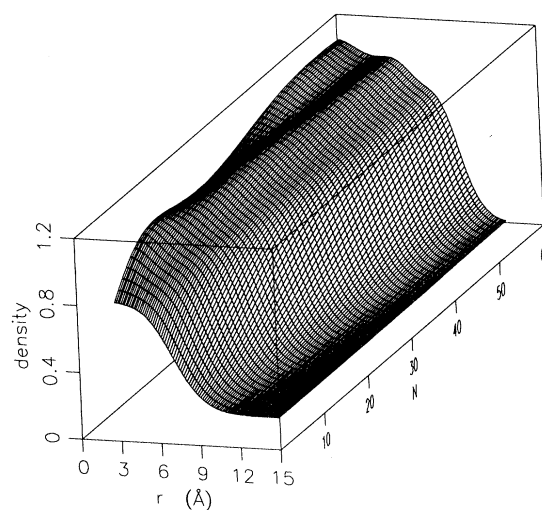


FIG. 5. Density profile of small ${}^4\text{He}$ droplets (density normalized to the bulk value).

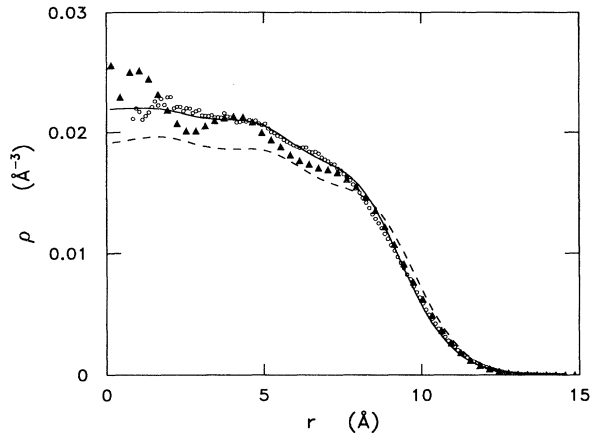


FIG. 6. Density profile of a droplet with 70 ^4He atoms. Solid line, present work; triangles, DMC simulations of Ref. 34; dashed line, variational (HNC) calculations (Ref. 35); circles, DMC simulation of Ref. 36.

calculations by Chin and Krotscheck.³⁴ An example is given in Fig. 6, where we show the density profile of a droplet with 70 particles. The solid line is the result of the present density-functional calculation, while the DMC results of Ref. 34 are represented by triangles. The DMC data exhibit more pronounced oscillations, but the presence of long-lived metastable states, slowing down the convergence in the Monte Carlo algorithm, cannot be completely ruled out.³⁴ Recently Chin and Krotscheck have found oscillations in $\rho(r)$ even with a variational approach based on the HNC approximation³⁵ (dashed line). Even though the HNC method underestimates the central density, it predicts oscillations with amplitude and phase in remarkable agreement with the ones of density-functional theory. An even better agreement is found in the most recent DMC calculations by Barnett and Whaley³⁶ (circles), where the statistical error is significantly reduced with respect to Ref. 34.

The detailed structure of $\rho(r)$, though interesting from a theoretical viewpoint, is not yet observable experimentally with enough accuracy to distinguish between a smooth profile and a profile with small oscillations. It is thus important to explore the effects of the soft sphere close packing on the energy systematics, since the latter is related to the mass distribution of droplets in the experimental beams.³⁷ In Fig. 7 the energy per particle is given as a function of N . The results of the present work (solid line) are compared with the ones of previous functionals (dashed and dotted lines), as well as with Monte Carlo simulations (dots from Ref. 34 and crosses from Ref. 38). First we note that the accuracy of the density functional theory, compared with *ab initio* simulations, increases progressively, following the improvement in the prediction of the static response function $\chi(q)$ in the microscopic region. The agreement between the results of our functional and Monte Carlo data is excellent. Second, as the energy is a smooth function of N , helium clusters behave essentially as liquid droplets. Indeed the energy can be easily fitted with a liquid drop formula:

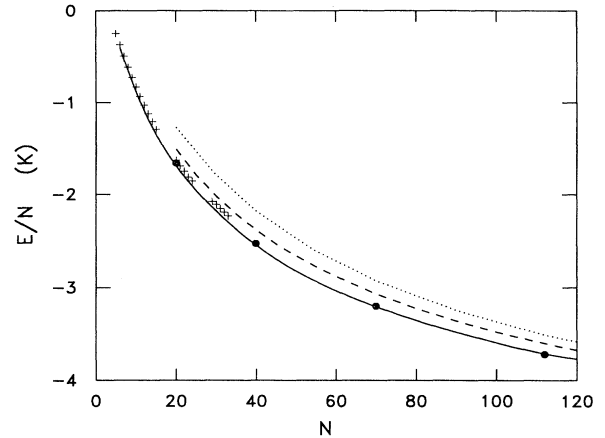


FIG. 7. Energy per particle versus N . Solid line, present work; dashed line, results with functional of Ref. 1; dotted line, Ref. 16; crosses, Ref. 38; circles, Ref. 34.

$$\frac{E}{N} = a_v + a_s N^{-1/3} + a_c N^{-2/3} + a_0 N^{-1} \quad , \quad (16)$$

where the volume coefficient a_v is the chemical potential in bulk and the surface energy a_s is fixed by the surface tension, while a_c and a_0 can be taken as fitting parameters. The energy calculated with the density functional differs from the liquid drop fit by less than 0.02 K for all droplets with $N > 30$. This seems to rule out apparently any shell effect in the energy systematics. However, the relevant quantity to investigate in this context is the evaporation energy $[E(N-1) - E(N)]$. The latter is not as smooth as the energy per particle. Figure 8 shows the evaporation energy predicted by the density-functional (solid line) and the one obtained with the liquid drop formula (16) (dashed line). The difference between the two curves is also shown (circles). When the difference is positive the droplets are more stable than is predicted

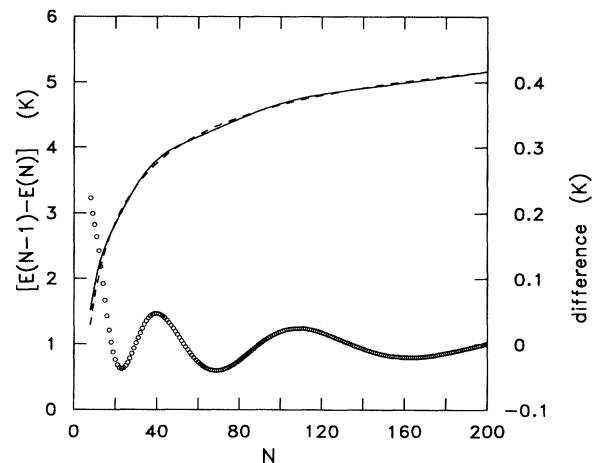


FIG. 8. Evaporation energy. Solid line, density functional; dashed line, liquid drop formula. Circles, deviation from the liquid drop formula (axis on the right).

TABLE I. Values of the potential parameters C_3 and D .

	Cs	Rb	K	Na	Li	Mg	Gr
C_3 (K \AA^3)	673	754	812	1070	1360	1775	2088
D (K)	4.41	4.99	6.26	10.4	17.1	32.1	192.6

by the liquid drop formula. We note clear oscillations, having decreasing amplitude and increasing periodicity as a function of N . The same kind of oscillations appear in the central density of the droplets, as seen in Fig. 5. Since the distance between two crests of the surface ripples is practically constant and the droplet radius goes approximately like $N^{1/3}$, the period of oscillations of the central density as a function of N , as well as the one of the evaporation energy, increases as $N^{1/3}$. The predicted deviations of the evaporation energy from the liquid drop behavior are rather small (less than 0.1 K). Unfortunately this value is smaller than the temperature of droplets in available experimental beams (about 0.4 K).

C. Layering and prewetting transitions in films

In order to find the equilibrium state of liquid helium on a solid substrate, we add the external helium-substrate potential $V_{\text{sub}}(\mathbf{r})$ to the mean field U in the Hartree equation (4). We assume the substrate to be flat, avoiding the problem of possible corrugations. This approximation is certainly valid for weak-binding substrates, such as the alkali metals, for which the cloud of delocalized electrons is expected to smooth out the potential along the substrate plane. In this case the Hartree equation is again one dimensional. The substrate-helium potential is taken here as a 9-3 potential of the form

$$V_{\text{sub}}(z) = \frac{4C_3^3}{27D^2z^9} - \frac{C_3}{z^3}, \quad (17)$$

where C_3 is the Hamaker constant and D the well depth of the potential. The values taken from Ref. 39 for various substrates are gathered in Table I.

The energetics of helium films on various surfaces indicate that two types of phase transition in film growth can take place, depending on the strength of the substrate potential. On strong and medium binding surfaces, which create large local pressures (one or two layers may become solid), the growth of the first liquid layers proceeds via *layering transitions*, described for helium on graphite in Ref. 40. When considering weak binding substrates, however, these layering transitions are no longer present. One enters a new regime of film adsorption where *prewetting transitions* take place at $T = 0$, as analyzed in detail in Ref. 4. By convention, the term layering transition is reserved usually to the case of a first-order transition in film thickness involving *one layer* only. The occurrence of such transition is not linked to the question of wetting; it is essentially related to the nature of the quasi-2D system. To the contrary, a prewetting transition involves a

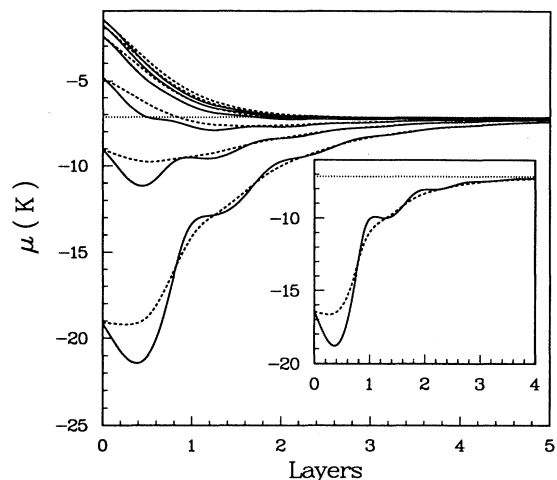


FIG. 9. Evolution of μ vs ${}^4\text{He}$ coverage on several substrates. Solid lines, present work; dashed lines, Orsay-Paris functional. The substrates are H_2 (inset) and, from top to bottom, Cs, Rb, K, Na, Li, Mg.

jump in film thickness which can take *any value*. The notion is intimately connected to that of wetting, since a prewetting transition is the continuation of the wetting transition off coexistence.

The various cases are best illustrated by considering, for a given substrate, the dependence of the chemical potential μ on coverage, as shown in Fig. 9. A negative slope ($d\mu/dN < 0$) indicates an unstable range of film thickness, and the transitions are determined by Maxwell constructions. The figure shows the results for a H_2 substrate and for the alkali metals. For H_2 , we have used a parametrization of the helium-substrate interaction proposed in Ref. 41:

$$V_{\text{H}_2}(z) = \frac{900\,000}{z^9} - \frac{15\,000}{z^5} - \frac{435}{z^3}, \quad (18)$$

where z is in \AA and V_{H_2} in K. This form is fitted to the results of Pierre *et al.*⁴² and gives a well depth of 33 K. The binding energy of one ${}^4\text{He}$ atom is 16.4 K, in good agreement with the experimental determination of Paine and Siedel,⁴³ which is 16 ± 2 K. For this potential, two layering transitions occur. The mechanism by which these transitions are produced can be summarized as follows: On a strong substrate, liquid helium forms well-defined layers which are approximately independent quasi-2D systems. As 2D helium is a liquid (Monte Carlo simulations⁴⁴ give a binding energy of 0.8 K at an equilibrium density of 0.043\AA^{-2}) the formation of each of the first layers exhibits a quasi-2D condensation. It is important to realize that the two aspects are necessary: On the one hand the layering transitions would not occur if quasi-2D ${}^4\text{He}$ were a gas; on the other hand we shall see below that they also disappear if the substrate is not strong enough to produce a sufficient layering of the fluid, as is the case with the alkalis. Figure 10 represents the growth of a helium film on H_2 characterized by two regions of instability or metastability.

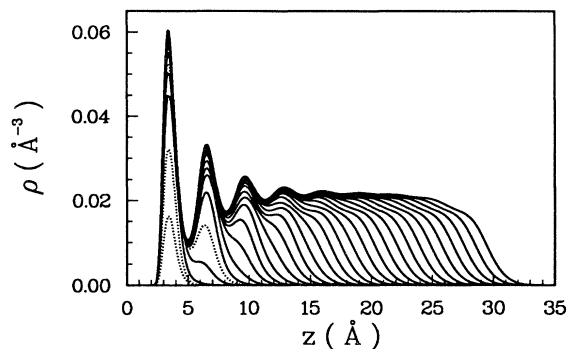


FIG. 10. Density profile of helium films on solid hydrogen from 0.02 to 0.6 \AA^{-2} . Solid lines, stable films; dotted lines, unstable or metastable films. The growth is not continuous because of the two layering transitions related to the formation of the first two layers.

One sees from Fig. 9 that the Orsay-Paris functional produces rather smooth curves and in particular misses the layering transitions besides the first one. This fact is due to two deficiencies of the model, related to the mechanism described above; namely, (i) the peak of the density-density response function $\chi(q)$ is underestimated, as we have seen, by a factor of almost 2 and (ii) the binding energy of the quasi-2D system is too small. Both deficiencies are corrected with the new functional.

Let us now turn to the results for the alkalis. Although $\mu(N)$ has still some structure, Mg appears as a limiting case where the layering transitions tend to disappear, except for the first one. Interestingly, one sees that with decreasing strength of substrate potential, it is this first transition which becomes larger and larger in amplitude and thus turns into the prewetting transition. The physics here is no longer that of the quasi-2D system, but that of wetting and prewetting: For a given substrate, the thinnest stable film is such that the energy cost of forming two interfaces—one with the substrate, one free surface—is compensated by the energy gain of placing the fluid in the attractive potential of the wall. The limit between wetted and nonwetted substrates is obtained when stability is obtained only for an infinitely thick film. Notice that the predictions of the Orsay-Paris functional and of the present one become similar for these weak binding surfaces. Using the original values of the substrate potential parameters, one still finds that the three alkalis Cs, Rb, and K are not wetted. The new functional slightly favors wetting with respect to the Orsay-Paris one. For example, the contact angle calculated for Cs is reduced by 3° ; also, on a Na substrate, the prewetting jump is reduced to 3.3 layers, compared to 5.2, and metastable films are found to exist down to 1.2 layers.

Layering growth can be also seen in the adsorption isotherms. In Fig. 11 is plotted the isotherm $T = 0.639$ K for helium on graphite. For comparison with experimental data⁴⁵ we use the ideal gas formula

$$\frac{P}{P_0} = \exp \left[\frac{\mu - \mu_0}{k_B T} \right], \quad (19)$$

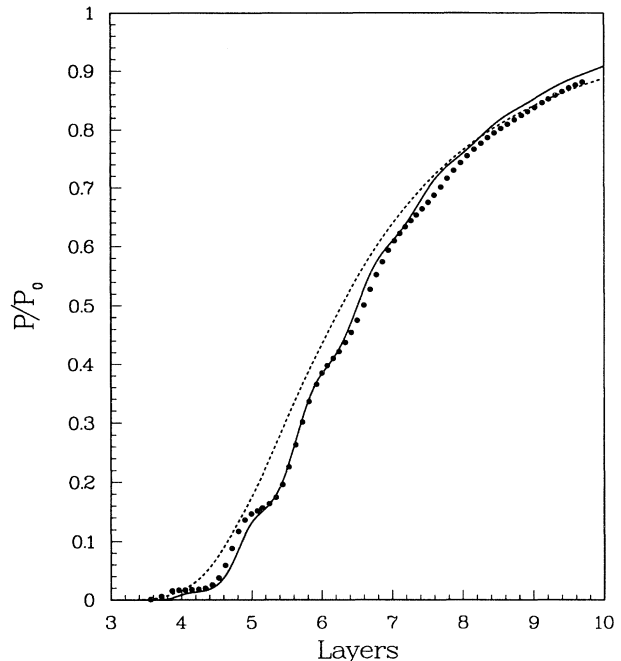


FIG. 11. Adsorption isotherm on a graphite substrate with $T = 0.639$ K. Solid line, present work; dashed lined, Orsay-Paris functional (Ref. 6); dots, experimental results extracted from Ref. 45. One layer corresponds to $0.078 \text{ 12 \AA}^{-2}$ (i.e., $\rho_0^{2/3}$ where ρ_0 is the bulk density).

where $\mu_0 = -7.15$ K is the bulk chemical potential and P_0 the saturating vapor pressure at T . The graphite substrate is a test for the model in a highly inhomogeneous situation. The two first layers are known to be solid. To first approximation, the effect of localization of the atoms in the plane parallel to the substrate can be ignored. Hence, we have treated the two solid layers as the liquid. The experimental data show a clear staircase structure, associated with the progressive filling of layers. The results of the present functional (solid line) exhibit a similar pattern, with steps of amplitude and phase close to the experimental ones.

IV. DYNAMICS

In Sec. II we wrote the Hartree equation (4) for the ground state of the fluid, which corresponds to the minimization of the energy E in Eq. (1) with respect to the density. This formalism is generalized to the study of dynamical properties using the least action principle:

$$\delta \int_{t_1}^{t_2} dt \int d\mathbf{r} \left[\mathcal{H}[\Psi^*, \Psi] - \mu \Psi^* \Psi - \Psi^* i \hbar \frac{\partial \Psi}{\partial t} \right] = 0. \quad (20)$$

The equations of motion for the excited states of the fluid can be derived by making variations with respect to Ψ or Ψ^* . One finds a Schrödinger-like equation of the form

$$(H - \mu)\Psi = i\hbar \frac{\partial}{\partial t} \Psi \quad , \quad (21)$$

where $H = \delta E / \delta \Psi^*$ is an effective Hamiltonian. We linearize the equation by writing

$$\Psi(\mathbf{r}, t) = \Psi_0(\mathbf{r}) + \delta\Psi(\mathbf{r}, t) \quad , \quad (22)$$

where $\Psi_0(\mathbf{r})$ refers to the ground state. The Hamiltonian H then takes the form

$$H = H_0 + \delta H \quad . \quad (23)$$

The static Hamiltonian

$$H_0 = -\frac{\hbar^2}{2m} \nabla^2 + U[\rho, \mathbf{r}] \quad , \quad (24)$$

which appeared already in Eq. (4), determines the equilibrium state $\Psi_0(\mathbf{r}) = \sqrt{\rho(\mathbf{r})}$. The term δH is linear in $\delta\Psi$ and accounts for changes in the Hamiltonian induced by the collective motion of the system. Since H depends explicitly on the wave function Ψ , the Schrödinger equation (21) has to be solved using a self-consistent procedure, even in the linear limit considered in the present work.

The formalism here described corresponds to a time-dependent density-functional (TDDF) theory which, in the linear limit (22), coincides with the random phase approximation (RPA) for a Bose system. This theory, which is basically a mean field theory coupling one-particle-one-hole configurations, is suitable for describing collective (one-phonon) states, but not multiphonons excitations.

A completely equivalent formulation of the equations of motion can be obtained by using the canonically conjugate variables ρ and S , defined in Eq. (2). The least action principle takes the form

$$\delta \int_{t_1}^{t_2} dt \int d\mathbf{r} \left[\mathcal{H}_0[\rho] + \mathcal{H}_v[\rho, \mathbf{v}] - \mu\rho + \rho \frac{\partial S}{\partial t} \right] = 0 \quad , \quad (25)$$

where we have separated the velocity-dependent part of the functional from the velocity-independent one. After variations with respect to ρ and S , one finds two coupled equations of the form

$$\frac{\partial \rho}{\partial t} + \frac{1}{m} \nabla_{\mathbf{r}} \cdot \frac{\delta}{\delta \mathbf{v}} \int d\mathbf{r} \{ \mathcal{H}_v[\rho, \mathbf{v}] \} = 0 \quad , \quad (26)$$

$$\frac{\partial S}{\partial t} + \frac{\delta}{\delta \rho} \int d\mathbf{r} \{ \mathcal{H}_0[\rho] + \mathcal{H}_v[\rho, \mathbf{v}] - \mu\rho \} = 0 \quad , \quad (27)$$

which can be viewed as a generalization of the equation of continuity and the Euler equation. In the hydrodynamic limit, \mathcal{H}_v is given by the usual kinetic energy term,

$$\mathcal{H}_v[\rho, \mathbf{v}] = \frac{m\rho}{2} |\mathbf{v}|^2 \quad , \quad (28)$$

so that (26) leads to the usual conserved current

$$\mathbf{J}_0(\mathbf{r}) = \rho(\mathbf{r})\mathbf{v}(\mathbf{r}) = \frac{\rho(\mathbf{r})}{m} \nabla S(\mathbf{r}) \quad . \quad (29)$$

The present formalism, with \mathcal{H}_v given by (28) and with different choices for \mathcal{H}_0 , has been already applied to helium droplets^{46,47} and films.⁹ However, there are two major shortcomings which make the results of those calculations not satisfactory from a quantitative point of view. First, the static response function is not well reproduced in the roton region. Second, the theory does not account for backflow effects.

To understand this point better, let us discuss the results of the TDDF in bulk. In this case the density is constant and $\delta\Psi$ can be expanded in plane waves, corresponding to the propagation of phonon-roton excitations. In the absence of backflow effects, the only dependence of the energy on the velocity field comes from the hydrodynamic limit of \mathcal{H}_v [see Eq. (28)] and the resulting dispersion relation for the phonon-roton mode takes the form

$$\hbar\omega(q) = \left(\frac{\hbar^2 q^2}{m|\chi(q)|} \right)^{1/2} \quad . \quad (30)$$

Result (30) can be also written in terms of the moments (8) of dynamic structure function $S(q, \omega)$. Indeed, one has

$$\hbar\omega(q) = \left(\frac{m_1(q)}{m_{-1}(q)} \right)^{1/2} \quad , \quad (31)$$

where the energy-weighted moment

$$m_1(q) = \int_0^\infty d\omega S(q, \omega) \hbar\omega = \frac{\hbar^2 q^2}{2m} \quad (32)$$

coincides with the well-known f -sum rule, while the inverse energy-weighted moment m_{-1} is related to the static response function by the compressibility sum rule (7).

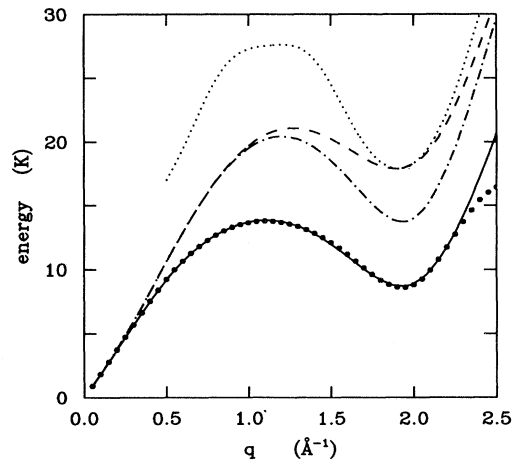


FIG. 12. Phonon-roton dispersion in bulk at zero pressure. Points, experimental data (Ref. 50); dotted line, Feynman approximation (33) with the experimental static form factor S_q (Ref. 51); dashed line, Orsay-Paris functional (Refs. 1, 9); dot-dashed line, from Eq. (20) with \mathcal{H}_v given in Eq. (28); solid line, same as before but with \mathcal{H}_v from Eq. (41).

Density functionals having the form (28) for \mathcal{H}_v exactly fulfill the f -sum rule. Thus, differences in the predictions for the dispersion $\omega(q)$ come only from the quantity $\chi(q)$, which is fixed by the static part $\mathcal{H}_0[\rho]$ of the functional. In Fig. 12 we show the results for the phonon-roton dispersion obtained with the Orsay-Paris functional (dashed line) and functional (9) (dot-dashed line). Both curves overestimate significantly the experimental phonon-roton energy (points). The difference between the predictions of the two functionals is clearly understood by looking at Fig. 1 and Eq. (30): Starting from the Hamiltonian density of Eq. (9), one obtains the full peak of $\chi(q)$ at the roton wavelength, thus predicting a lower roton energy. The remaining gap between theory and experiment is mainly due to the role of multiphonon excitations in the f -sum rule. In fact, the analysis of the spectra of neutron scattering experiments²⁰ shows that the collective mode gives only a fraction ($\simeq 1/3$) to the f -sum rule in the roton region, the remaining part being exhausted by high-energy multiphonon excitations. On the contrary, due to the ω^{-1} factor in the integrand, the collective mode almost exhausts the compressibility sum rule for wavelengths up to about 2.2 \AA^{-1} . This means that in order to have an accurate prediction for $\omega(q)$, only the single-mode contribution to the f -sum rule should be included in the moment $m_1(q)$ entering Eq. (31). Therefore, one concludes that, once the static response function $\chi(q)$ is properly accounted for, the dispersion law (30) given by TDDF theory provides an upper bound to the exact energy of the phonon-roton mode.

It is instructive to compare the above predictions with the results of the so called Feynman approximation for collective excitations,⁴⁸ often used in dynamic calculations for nonuniform ^4He states.^{13,33,34,49} In the bulk the Feynman dispersion law takes the form

$$\hbar\omega_F(q) = \frac{m_1(q)}{m_0(q)} = \frac{\hbar^2 q^2}{2mS_q} \quad , \quad (33)$$

where the static structure factor is related to the non-energy-weighted moment of $S(q, \omega)$ through the equation

$$S(q) = m_0(q) = \int d\omega S(q, \omega) \quad . \quad (34)$$

General properties of the moments m_n permit one to

prove the following inequality:

$$\sqrt{\frac{m_1}{m_{-1}}} \leq \frac{m_1}{m_0} \quad , \quad (35)$$

holding at zero temperature. This implies that the dispersion law given by Eqs. (30), (31) provides an upper bound closer to the exact dispersion law with respect to the Feynman approximation. This is explicitly shown in Fig. 12.

Concerning the static structure factor $S(q)$, one should note that it cannot be properly accounted for by the TDDF theory developed above. The reason is that, in the bulk liquid, this theory represents a single-mode approximation with the dynamic structure function in the form

$$S^{\text{DF}}(q, \omega) = \frac{\hbar q^2}{2m\omega_{\text{DF}}} \delta(\omega - \omega_{\text{DF}}) \quad (36)$$

and the dispersion law ω_{DF} given by Eq. (31). While Eq. (36) reproduces exactly the sum rules m_1 and m_{-1} , it yields the approximate expression

$$S^{\text{DF}}(q) = \sqrt{m_1(q)m_{-1}(q)} = \sqrt{\frac{\hbar^2 q^2}{4m} |\chi(q)|} \quad (37)$$

for the static structure factor. Actually result (37) provides an upper bound to the exact value of $S(q)$. The difference is again due to the role of multiphonon excitations.

One of the purposes of this work is to make the TDDF theory more quantitative. The idea is to realize that the expression of \mathcal{H}_v given by Eq. (28) comes from a many-body wave function of the form

$$\Psi_N(\mathbf{r}_1, \dots, \mathbf{r}_N) = \exp \left[i \sum_i s(\mathbf{r}_i) \right] |\Psi_N(\mathbf{r}_1, \dots, \mathbf{r}_N)| \quad , \quad (38)$$

where s is real. Clearly, this wave function does not take into account short-range phase correlation, and describes correctly the superfluid motion in the hydrodynamic limit only. The exact wave function should be expressed with a more general phase:

$$s(\mathbf{r}_1, \mathbf{r}_2, \dots, \mathbf{r}_N) = \sum_i s_1(\mathbf{r}_i) + \sum_{i<j} s_2(\mathbf{r}_i, \mathbf{r}_j) + \dots + \sum_{i<j<k\dots} s_N(\mathbf{r}_i, \mathbf{r}_j, \mathbf{r}_k, \dots) \quad . \quad (39)$$

The average kinetic energy obtained from this wave function has nonlocal contributions coming from s_2, \dots, s_N . Now, if we make the assumption that those terms can be expressed only with the two canonically conjugate variables ρ and S , then we are led to add a nonlocal velocity-dependent term to $\mathcal{H}_v[\rho, \mathbf{v}]$. Indeed, this procedure was proposed a long time ago by Thouless¹⁰ in the study of the flow of a dense superfluid, but in his article, helium was treated as an incompressible liquid. In the present work, we incorporate the suggestion of Thouless by introducing the most general quadratic form

$$\mathcal{H}_v = \frac{m}{2} \rho(\mathbf{r}) |\mathbf{v}(\mathbf{r})|^2 + \int d\mathbf{r}_1 d\mathbf{r}_2 d\mathbf{r}_3 [\mathbf{v}(\mathbf{r}) - \mathbf{v}(\mathbf{r}_1)] \underline{G}(\rho; \mathbf{r}, \mathbf{r}_1, \mathbf{r}_2, \mathbf{r}_3) [\mathbf{v}(\mathbf{r}_2) - \mathbf{v}(\mathbf{r}_3)] \quad , \quad (40)$$

where we have explicitly exhibited Galilean invariance. Generally speaking, \underline{G} is a tensor which takes nonzero values

TABLE II. Values of the parameters used in $V_J(\mathbf{r})$; see Eq. (46).

γ_{11}	γ_{21}	γ_{12}	γ_{22}	α_1	α_2
-19.7544	-0.2395	12.5616 \AA^{-2}	0.0312 \AA^{-2}	1.023 \AA^{-2}	0.14912 \AA^{-2}

on scales $|\mathbf{r}_i - \mathbf{r}_j|$ of the order of the interparticle distance. So far no microscopic derivation has been found for this functional form. Our phenomenological approach consists in keeping only diagonal terms as follows:

$$\mathcal{H}_v = \frac{m}{2} \rho(\mathbf{r}) |\mathbf{v}(\mathbf{r})|^2 - \frac{m}{4} \int d\mathbf{r}' V_J(|\mathbf{r} - \mathbf{r}'|) \rho(\mathbf{r}) \rho(\mathbf{r}') [\mathbf{v}(\mathbf{r}) - \mathbf{v}(\mathbf{r}')]^2, \quad (41)$$

and fixing the effective current-current interaction V_J to reproduce known properties in bulk. The new term plays the role of a nonlocal kinetic energy. Now, the conserved current is no longer \mathbf{J}_0 ; rather, Eq. (26) leads to the current

$$\mathbf{J}(\mathbf{r}) = \mathbf{J}_0(\mathbf{r}) + \mathbf{J}_B(\mathbf{r}), \quad (42)$$

$$\mathbf{J}_B(\mathbf{r}) = \rho(\mathbf{r}) \int \rho(\mathbf{r}') [\mathbf{v}(\mathbf{r}) - \mathbf{v}(\mathbf{r}')] V_J(|\mathbf{r} - \mathbf{r}'|) d\mathbf{r}'. \quad (43)$$

Physically, $\mathbf{J}_B(\mathbf{r})$ acts as a backflow which depends on the velocity and the density in the vicinity of point \mathbf{r} . As expected, its contribution vanishes when many-body phenomena are not present ($\rho \rightarrow 0$).

This form of \mathcal{H}_v lowers the value of the energy-weighted moment $m_1(q)$ predicted by the density-functional theory. In bulk one now finds

$$m_1(q) = \frac{\hbar^2 q^2}{2m} \left\{ 1 - \rho \left[\hat{V}_J(0) - \hat{V}_J(q) \right] \right\}, \quad (44)$$

where $\hat{V}_J(q)$ is the Fourier transform of the current-current interaction $V_J(r)$. Notice that the expression for the static response function $\chi(q)$ does not change, since it is entirely fixed by \mathcal{H}_0 . The phonon-roton dispersion in bulk is still given by the ratio (31), so that the dispersion law is given by

$$[\hbar\omega(q)]^2 = \frac{\hbar^2 q^2}{m|\chi(q)|} \left\{ 1 - \rho \left[\hat{V}_J(0) - \hat{V}_J(q) \right] \right\}. \quad (45)$$

This relation can be used to fix $V_J(r)$ in order to reproduce phenomenologically the experimental phonon-roton dispersion. We have chosen the simple parametrization

$$V_J(r) = (\gamma_{11} + \gamma_{12}r^2) \exp(-\alpha_1 r^2) + (\gamma_{21} + \gamma_{22}r^2) \exp(-\alpha_2 r^2), \quad (46)$$

where the parameters are given in Table II. The corresponding dispersion relation is shown in Fig. 12 (solid line). The roton minimum is at $q_0 = 1.92 \text{\AA}^{-1}$ and the roton energy is $\Delta = 8.7 \text{ K}$. The pressure dependence of the dispersion relation turns out to be also well repro-

duced. At $P = 24 \text{ atm}$, for instance, the roton minimum is displaced at $q = 2.01 \text{\AA}^{-1}$ and the roton energy is $\Delta = 7.4 \text{ K}$, close to the experimental values $q = 2.05 \text{\AA}^{-1}$ and $\Delta = 7.3 \text{ K}$.⁵²

The energy-weighted moment $m_1(q)$ is shown in Fig. 13, where the density-functional result (44) is compared with the experimental data for the collective contribution to the f -sum rule.²⁰ The fact that the new functional no longer satisfies the f -sum rule (32) points out in a clear way that the TDDF theory does not account for multiphonon excitations. The new current-current term in the functional (41) changes also the expression for the static structure factor, which is still given by $S^{\text{DF}}(q) = \sqrt{m_1(q)m_{-1}(q)}$ as in Eq. (37), but with the new $m_1(q)$ moment (44). The resulting $S^{\text{DF}}(q)$ is no longer an upper bound to the exact $S(q)$; conversely it turns out to be close to the experimental one-phonon contribution to the total $S(q)$. A similar separation between collective and multiphonon excitations, in the context of linear response theory, has been developed by Pines.⁵³ Finally we note that the dispersion law (45) is not affected by the new term in the $q \rightarrow 0$ hydrodynamic regime, where it gives the usual sound velocity $c^2 = -[m\chi(0)]^{-1}$. This is an important feature ensured by Galilean invariance.

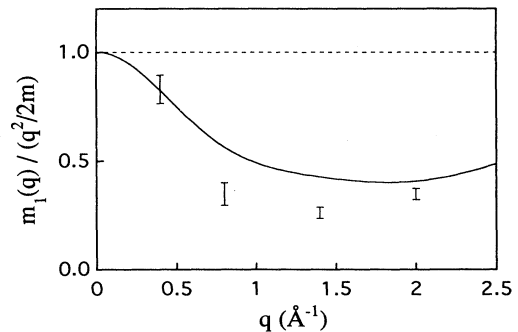


FIG. 13. Energy-weighted moment of the dynamic structure function. Dashed line, total f -sum rule; bars, one-phonon contribution as measured in neutron scattering (Ref. 20); solid line, present work [Eq. (44)].

In conclusion, the complete Orsay-Trento functional has the form

$$E = \int d\mathbf{r} \{ \mathcal{H}_0[\rho] + \mathcal{H}_v[\rho, \mathbf{v}] \} , \quad (47)$$

where \mathcal{H}_0 and \mathcal{H}_v are given in Eqs. (9) and (41), respectively. The term \mathcal{H}_v vanishes in the ground state calculations of the previous sections. On the contrary, it is crucial in the calculation of the dynamics. Both the experimental static response function and the phonon-roton dispersion in bulk are taken as input to parametrize the functional. The theory can then be applied to study the excited states of inhomogeneous systems. This is the purpose of the next section.

V. EXCITED STATES OF THE FREE SURFACE AND FILMS

A. Equations of motion

A detailed study of excitations using the Orsay-Paris functional can be found in Ref. 9. The same method of resolution is followed here. The systems under consideration have translational invariance parallel to the x - y plane; hence the ground state wave function depends only on one coordinate, which is taken as the z coordinate orthogonal to the free surface or to the plane of a film. The excited state wave functions can be expanded in plane waves as follows:

$$\Psi(\mathbf{r}_{\parallel}, z, t) = \Psi_0(z) + \sum_{\mathbf{k}, b} \frac{1}{\sqrt{AL}} \{ \alpha_{\mathbf{k}, b} \Phi_{\mathbf{k}, b}^1(z) e^{-i(\omega_{\mathbf{k}, b} t - \mathbf{k} \cdot \mathbf{r}_{\parallel})} + \alpha_{\mathbf{k}, b}^* \Phi_{\mathbf{k}, b}^2(z) e^{i(\omega_{\mathbf{k}, b} t - \mathbf{k} \cdot \mathbf{r}_{\parallel})} \} , \quad (48)$$

where \mathbf{r}_{\parallel} denotes from now on a two-dimensional vector parallel to the surface of the liquid. The quantities $\alpha_{\mathbf{k}, b}$ are small amplitudes, the factor $1/\sqrt{AL}$ is a normalization constant (A is the area of the sample, L is an arbitrary length), and b labels the various branches of excited states. The functions $\Phi_1(z)$ and $\Phi_2(z)$, without any loss of generality, can be chosen as real. This formalism has been already used in Refs. 9, 18.

It is convenient to introduce the quantities

$$\Phi_{\mathbf{k}, b}^{\pm} = \Phi_{\mathbf{k}, b}^1 \pm \Phi_{\mathbf{k}, b}^{2*} . \quad (49)$$

Then the phase S can be written as

$$S(\mathbf{r}_{\parallel}, z, t) = -\frac{i\hbar}{2\sqrt{AL}} \sum_{\mathbf{k}, b} \frac{1}{\Psi_0(z)} \{ \alpha_{\mathbf{k}, b} \Phi_{\mathbf{k}, b}^-(z) e^{-i(\omega_{\mathbf{k}, b} t - \mathbf{k} \cdot \mathbf{r}_{\parallel})} \} + \text{c.c.} \quad (50)$$

and the density takes the form

$$\rho(\mathbf{r}_{\parallel}, z, t) = \rho_0(z) + \delta\rho(\mathbf{r}_{\parallel}, z, t) , \quad (51)$$

where $\rho_0 = |\Psi_0|^2$ is the ground state density, while

$$\delta\rho(\mathbf{r}_{\parallel}, z, t) = \frac{1}{\sqrt{AL}} \sum_{\mathbf{k}, b} \Psi_0(z) \{ \alpha_{\mathbf{k}, b} \Phi_{\mathbf{k}, b}^+(z) e^{-i(\omega_{\mathbf{k}, b} t - \mathbf{k} \cdot \mathbf{r}_{\parallel})} \} + \text{c.c.} \quad (52)$$

The equations of motion (26) and (27) assume the form

$$\begin{aligned} \mathcal{D}_k \Phi_{\mathbf{k}, b}^+ + \mathcal{W} \{ \Phi_{\mathbf{k}, b}^+ \} &= \hbar\omega_{\mathbf{k}, b} \Phi_{\mathbf{k}, b}^-, \\ \mathcal{D}_k \Phi_{\mathbf{k}, b}^- + \mathcal{U} \{ \Phi_{\mathbf{k}, b}^- \} &= \hbar\omega_{\mathbf{k}, b} \Phi_{\mathbf{k}, b}^+ . \end{aligned} \quad (53)$$

The eigenvalues $\hbar\omega_{\mathbf{k}, b}$ satisfying Eq. (53) are the energies of the collective modes of the system. The symbol \mathcal{D}_k denotes a differential operator of second order, while \mathcal{W} and \mathcal{U} are integral operators. They are defined by

$$\mathcal{D}_k = -\frac{\hbar^2}{2m} \frac{d^2}{dz^2} + \frac{\hbar^2 k^2}{2m} + U[\rho_0, z] + V_{\text{sub}}(z) - \mu , \quad (54)$$

$$\mathcal{W}\{f\} = 2\Psi_0(z) \int d\mathbf{r}' \Psi_0(z') f(z') \left[\frac{\delta^2 E_c}{\delta\rho(\mathbf{r})\delta\rho(\mathbf{r}')} \right] e^{i\mathbf{k} \cdot (\mathbf{r}_{\parallel} - \mathbf{r}'_{\parallel})} , \quad (55)$$

$$\mathcal{U}\{f\} = \frac{1}{2\Psi_0(z)} \int d\mathbf{r}' \frac{f(z')}{\Psi_0(z')} \left[\frac{\delta^2 E_v}{\delta S(\mathbf{r})\delta S(\mathbf{r}')} \right] e^{i\mathbf{k} \cdot (\mathbf{r}_{\parallel} - \mathbf{r}'_{\parallel})} , \quad (56)$$

where E_v is a functional containing only the nonlocal part of \mathcal{H}_v . A simple way of solving Eq. (53) is to expand it on the basis of eigenstates of the static one-body Hamiltonian. This leads to a matrix equation that is easily solved numerically by a direct diagonalization.

A quantum hydrodynamical formalism is also obtained by making the substitution $\{-i\alpha_{\mathbf{k},b}\} \rightarrow a_{\mathbf{k},b}$, where $a_{\mathbf{k},b}$ is the operator of creation of one phonon which satisfies the Bose commutation rules

$$[a_{\mathbf{k},b}, a_{\mathbf{k}',b'}^\dagger] = \delta_{\mathbf{k},\mathbf{k}'} \delta_{b,b'} , \quad [a_{\mathbf{k},b}, a_{\mathbf{k}',b'}] = 0 . \quad (57)$$

From the completeness relation

$$\sum_b \Phi_{k,b}^-(z) \Phi_{k,b}^+(z') = L \delta(z - z') , \quad (58)$$

one recovers the equalities

$$[\rho(\mathbf{r}), S(\mathbf{r}')] = i\hbar \delta(\mathbf{r} - \mathbf{r}') , \quad [\rho(\mathbf{r}), \rho(\mathbf{r}')] = [S(\mathbf{r}), S(\mathbf{r}')] = 0 . \quad (59)$$

Then, after a quadratic expansion of the total energy and using the properties of Eq. (53), one finds the Hamiltonian

$$H^{(2)} = E_0 + \sum_{\mathbf{k},b} \hbar \omega_{\mathbf{k},b} a_{\mathbf{k},b}^\dagger a_{\mathbf{k},b} , \quad (60)$$

where E_0 is the energy of the ground state. This diagonalization is obtained provided the $\Phi_{k,b}^\pm$'s are normalized according to

$$\int dz \Phi_{k,b}^-(z) \Phi_{k,b'}^+(z) = L \delta_{b,b'} , \quad (61)$$

where the orthogonality appears as a consequence of (53). Higher-order expansions of H in terms of density and phase fluctuations would give rise to interactions between quasiparticles.

The transition density associated with the solution (52) is given by [the vector \mathbf{q} denotes (\mathbf{k}, q_z)]

$$(\rho_{\mathbf{q}}^\dagger)_{\mathbf{k},b} = -i \sqrt{\frac{A}{L}} \int \Psi_0(z) \Phi_{k,b}^+(z) \exp(iq_z z) dz , \quad (62)$$

and the dynamic structure function can be evaluated by means of the definition

$$S(k, q_z, \omega) = \sum_b \left| (\rho_{\mathbf{q}}^\dagger)_{\mathbf{k},b} \right|^2 \delta(\omega - \omega_{\mathbf{k},b}) . \quad (63)$$

In order to compare the theoretical strength with the experimental results, we have introduced a width of the order of the experimental resolution, by substituting the δ function of Eq. (63) with a normalized Gaussian, as done in Ref. 54.

B. Dynamics of the free surface

We have done calculations in a slab geometry, i.e., liquid between two parallel surfaces at a distance L much larger than the surface thickness (typically 50 – 100 Å). The slab geometry is a good approximation to a semi-infinite medium for wave vectors larger than $1/L$. The dispersion relation of the various modes, extrapolated to

$L \rightarrow \infty$, are shown in Fig. 14. The lowest branch corresponds to a wave function $\Phi^+(z)$ localized in the surface region. In the long-wavelength limit, it coincides with the hydrodynamical surface wave called ripplon, whose dispersion is

$$\omega^2(k) = \frac{\sigma k^3}{m \rho_\infty} , \quad (64)$$

where σ and ρ_∞ are the surface tension and the bulk density, respectively. For wave vectors of the order of 0.5 \AA^{-1} , the dispersion relation starts deviating from the hydrodynamical limit, until its curvature eventually changes sign, due to a coupling with bulk modes. Our curve reaches the value of the roton energy $\Delta = 8.7 \text{ K}$ at about $k = 1.15 \text{ \AA}^{-1}$. A first experimental evidence of a similar deviation from the hydrodynamic law came from measurements of the surface entropy.⁵⁵ More recently the dispersion of surface modes has been measured

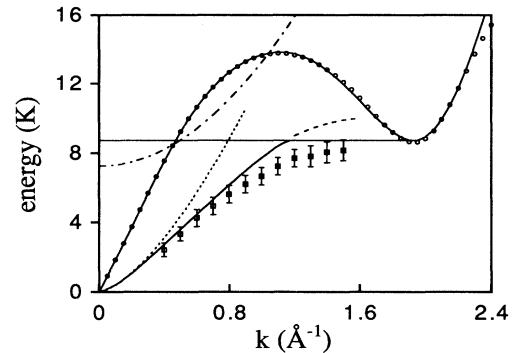


FIG. 14. Dispersion relation of bulk and free surface excitations. The threshold $\Delta = 8.7 \text{ K}$, for roton states with different values of parallel wave vector k , is shown as the horizontal line. The present result for the surface mode (lowest solid line reaching Δ at $k = 1.15 \text{ \AA}^{-1}$) is compared with the experimental data on films (Ref. 56) (squares) and with the hydrodynamic dispersion of ripples (short-dashed line). The bulk phonon-roton branch (upper solid line) is compared with the experimental one (circles). The threshold for the emission of atoms into the vacuum is also shown (dot-dashed curve).

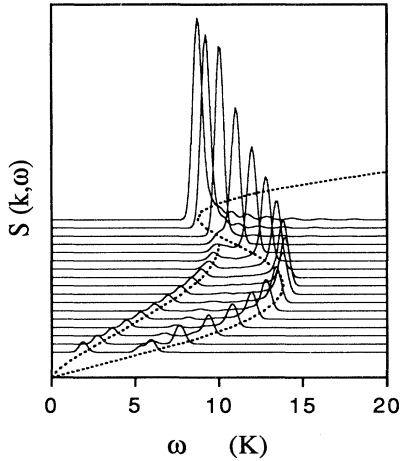


FIG. 15. Dynamic structure function (in arbitrary units) for $q_z = 0$ in a slab 50 Å thick. The lowest line corresponds to $k = 0.3 \text{ \AA}^{-1}$, the highest one to $k = 1.9 \text{ \AA}^{-1}$. The dashed lines are the phonon-roton and the ripplon dispersion. The δ function in the definition (63) is replaced by a Gaussian of width 0.4 K.

in neutron scattering experiments on helium films.⁵⁶ The experimental data are shown in Fig. 14 as squares, the error bars accounting for the spreading of the data for different coverages (3.5 – 5 layers of helium on graphite). The agreement with the calculated values is satisfactory.

Below Δ the surface modes are undamped, while above Δ they couple with the continuum of bulk modes (rotons with negative and positive group velocity) propagating at different angles ($q_z \neq 0$). This results in a spreading of the strength associated with the surface modes. Actually the spreading predicted by our theory is small. In Fig. 15 we show the dynamic structure function for scattering at grazing angle ($q_z = 0$) on a slab of thickness $L = 50 \text{ \AA}$. The strength of the lowest surface mode is well localized not only below but also above Δ , even though it is partially distributed among bulk modes coupled to ripples. The position of the peak of the ripplon mode above Δ is shown also in Fig. 14 as a dashed line.

We obtain also a second branch of surface excitations, lying in between the ripplon and the phonon-roton modes. It is visible in Fig. 15 as a small bump, which is close to the phonon peak for $k \simeq 0.3 \text{ \AA}^{-1}$, and stays almost parallel to the ripplon dispersion for larger k . The relative strength of this mode is larger in thin films; in that case, the experiments seem also to support the existence of such a surface mode.

A more detailed analysis of the results of the present density-functional theory for the excitations of the free surface is given in Ref. 57; in that work, a general discussion of the mechanism of hybridization between ripples and rotons is presented, and some properties connected with reflection and evaporation of bulk excitations impinging on the surface are also discussed.

C. Dynamics of films

In order to illustrate the results obtained with the present model, we have chosen the case of a H_2 substrate, since it has been the subject of both experimental and theoretical investigations.^{6,58} Besides finite-size effects, the interesting features to be expected are linked to the layering of the liquid near the substrate. Submonolayer superfluidity has been observed on H_2 ,⁵⁸ indicating that helium remains liquid close to the substrate. However, the well depth of the helium-hydrogen potential is rather large (33 K), which produces a well defined layering of the liquid.

In a thin film, the long-wavelength limit of the lowest surface mode is no longer a ripplon, for which the restoring force originates from the surface tension, but rather a third-sound excitation. The restoring force is here given by the substrate potential. The third-sound speed c_{3s} is obtained as the hydrodynamic limit ($\mathbf{k} \rightarrow 0$) of Eq. (53):

$$mc_{3s}^2 = N \frac{d\mu}{dN}, \quad (65)$$

where N is the coverage of the film. Indeed, one can verify that for small momentum, $\Phi^- \sim \Psi_0$, so that the contribution due to \mathcal{U} vanishes. With increasing film thickness, since the chemical potential varies as $1/N^3$, so does c_{3s}^2 .

The results for c_{3s} (Fig. 16), show strong oscillations as a function of coverage. This is due to the layered structure of the film, which is reflected into the coverage dependence of the chemical potential (see Sec. III C

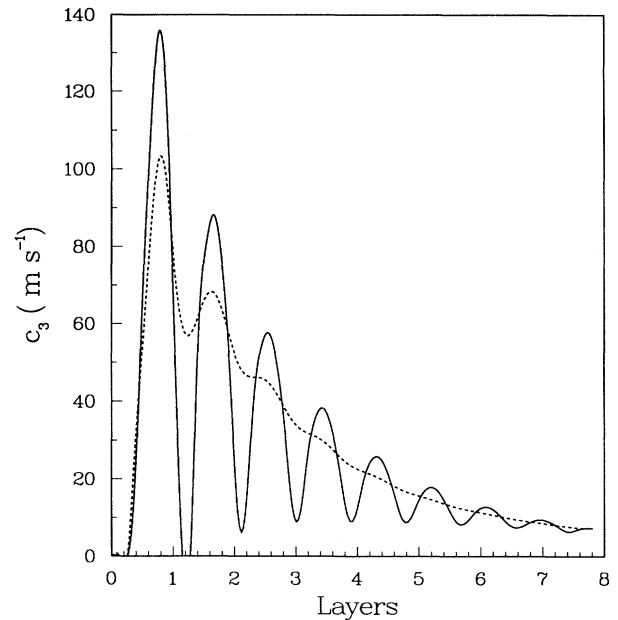


FIG. 16. Evolution of third sound speed c_{3s} vs coverage on a H_2 substrate. Solid line, Orsay-Trento results. Dashed line, Orsay-Paris results.

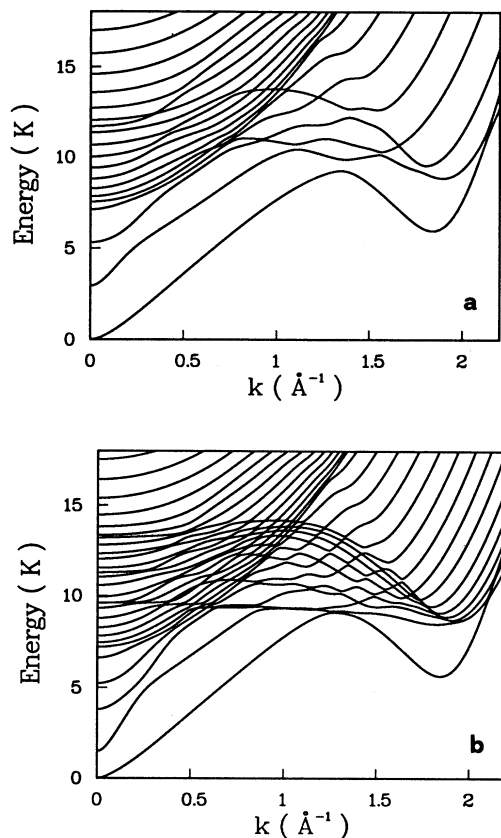


FIG. 17. Spectrum of films on a H_2 substrate for coverages 0.24 \AA^{-2} (a) and 0.48 \AA^{-2} (b). Note the presence of a low-energy excitation around 2 \AA^{-1} which is associated with a 2D roton mode trapped in the first layer.

above). Films for which a uniform coverage is unstable have a constant chemical potential characteristic of a layering transition, the range of which is determined by a Maxwell construction as discussed above. This causes the third-sound velocity to drop dramatically to zero. The structure is more marked than with the Orsay-Paris functional,⁶ which missed the layering transitions besides the first one (see Sec. III C). Experimentally, there has been up to now no indication of the layering transitions. The third-sound velocity does show oscillations,⁵⁸ however less marked than calculated here, although the measurements were done at a temperature of 0.18 K, which is expected to be lower than the critical temperature of the layering transitions. It is also possible that surface inhomogeneities of the H_2 surface are able to smooth out the dips seen in the calculations of c_{3s} for a perfectly flat surface.

Two typical spectra are shown in Fig. 17 for two values of helium coverage ($N = 0.24 \text{ \AA}^{-2}$ and $N = 0.48 \text{ \AA}^{-2}$) on a H_2 substrate. For wave vectors in the range $1.5 - 2 \text{ \AA}^{-1}$, the low-lying excited states are modes confined in the first layers of the fluid close to the substrate. Their nature has been discussed in details in Refs. 9 and 54. Their formation reflects the fact that the substrate-

liquid interface is nearly solidified, so that low-energy excitations appear, trapped in each of the first layers, with a momentum corresponding to the interparticle distance. The minimum 2D roton energy was found to be about 12 K with the Orsay-Paris functional. It reduces to 5.6 K with the present one. The combined effect of the evolution of the third-sound excitation and of the 2D roton, with completion of the first layer, may lead to unexpected behavior of the heat capacity of submonolayer films.⁹

In Fig. 18, we show the dynamic structure function associated with the spectra of Fig. 17. The strength distribution of the thinner film is more fragmented, as an effect of the finite size of the system in the z direction.

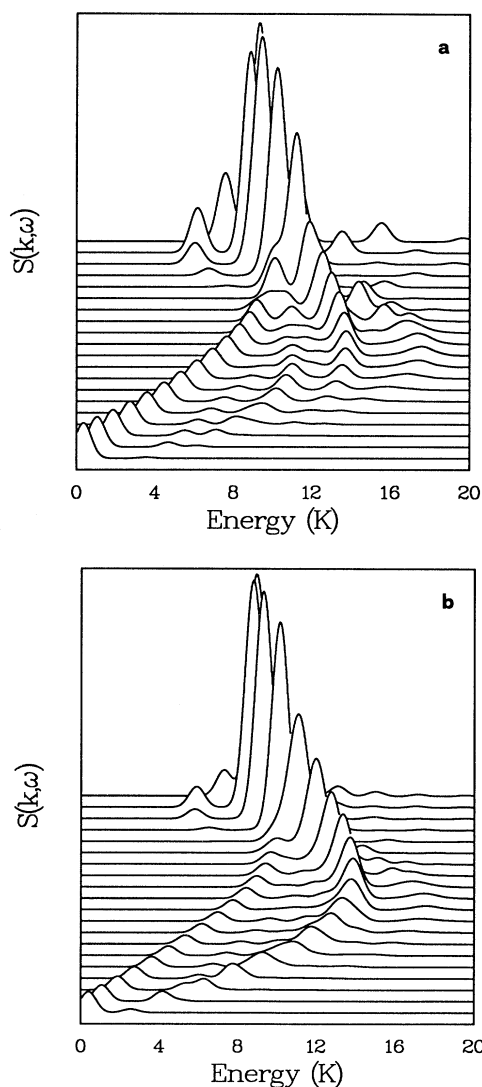


FIG. 18. Dynamic structure function (in arbitrary units) associated with the spectra in Fig. 17, for coverages 0.24 \AA^{-2} (a) and 0.48 \AA^{-2} (b) on a H_2 substrate. The lowest line corresponds to $k = 0.1 \text{ \AA}^{-1}$, the highest one to $k = 2.0 \text{ \AA}^{-1}$. The δ function in the definition (63) is replaced by a Gaussian of width 0.4 K.

The relative strength of the ripplon mode is also higher for the thinner film, since the surface-to-volume ratio is larger. One notes also that the surface mode maintains its identity well above the roton energy. The thicker film has a spectrum quite similar to the one of the free surface, apart from the 2D roton at the substrate-helium interface, which is still present but affects the spectrum only in the region $q \simeq 2 \text{ \AA}^{-1}$. The spectrum is dominated by the bulk phonon-roton mode and the lowest surface mode, a non-negligible strength being also associated with the excited surface modes which lie in between.

It is worth noticing that the potential between one ^4He atom and the H_2 substrate is similar to that between one ^4He and a graphite substrate coated by two solid ^4He layers.^{54,59} Hence, the liquid ^4He film on graphite has a spatial structure similar to the profile of Fig. 10. Thus we can safely compare our results with the experimental ones, obtained at ILL-Grenoble,⁵⁶ as well as with the variational theory of Ref. 59. The spectra in Fig. 17 are indeed similar to the experimental ones (see, for example, Fig. 14 of Ref. 59). The energy of the excitations are in rather good agreement, apart from the energy of the 2D roton which, however, depends crucially on the substrate-helium potential. A reasonable agreement is also obtained for the strength distribution.

VI. CONCLUSIONS

We have presented a density-functional theory for liquid ^4He at zero temperature. The theory corresponds to an improved version of the density functional introduced in Ref. 1. It is a phenomenological theory, where known properties of the uniform liquid are used to fix the parameters of the functional. The theory is suitable to study

inhomogeneous states of liquid helium in different geometries like the free surface, droplets, films, bubbles, and vortices. Equilibrium configurations and excited states can be studied in a unified framework. Here we have presented results for static and dynamic properties of the free surface and films, as well as for the ground state of helium droplets. The comparison with available experimental data, as well as with Monte Carlo simulations, is in general satisfactory. The present density-functional theory turns out to be quantitative even on the scale of interatomic distances. The improvements with respect to previous density functionals are clearly understood in term of the key ingredients of the theory, namely, (i) the bulk equation of state; (ii) the static response function and (iii) the phonon-roton dispersion in the uniform liquid. In particular we have discussed in detail the importance of reproducing the peak of the static response function at the roton wavelength in determining static density oscillations near the surface and shell structures in helium droplets. We have also discussed the contribution of the collective (one-phonon) modes to sum rules (compressibility sum rule, f -sum rule, static form factor), in order to clarify the grounds of TDDF theory, as well as to include backflow effects. The results for the excited states of the free surface and films compare quantitatively with experiments. The applications of the same theory to the dynamics of droplets and to the phenomenon of quantum evaporation are work in progress.

ACKNOWLEDGMENTS

We are indebted to L. Pitaevskii for many useful discussions. This work was partially supported by European Community Grant No. ERBCHRXCT920075.

¹ J. Dupont-Roc, M. Himbert, N. Pavloff, and J. Treiner, *J. Low Temp. Phys.* **81**, 31 (1990).

² N. Pavloff and J. Treiner, *J. Low Temp. Phys.* **83**, 331 (1991)

³ J. Treiner, *J. Low Temp. Phys.* **92**, 1 (1993).

⁴ E. Cheng, M.W. Cole, W.F. Saam, and J. Treiner, *Phys. Rev. Lett.* **67**, 1007 (1991); *Phys. Rev. B* **46**, 13 967 (1992); **47**, 14 661(E) (1993).

⁵ E. Cheng, M.W. Cole, J. Dupont-Roc, W.F. Saam, and J. Treiner, *Rev. Mod. Phys.* **65**, 557 (1993).

⁶ E. Cheng, M.W. Cole, W.F. Saam, and J. Treiner, *J. Low Temp. Phys.* **92**, 10 (1993).

⁷ F. Dalfovo, *Phys. Rev. B* **46**, 5482 (1992); F. Dalfovo, G. Renversez, and J. Treiner, *J. Low Temp. Phys.* **89**, 425 (1992).

⁸ F. Dalfovo, *Z. Phys. D* **29**, 61 (1994).

⁹ L. Pricauenko and J. Treiner, *J. Low Temp. Phys.* **96**, 19 (1994).

¹⁰ D.J. Thouless, *Ann. Phys. (N.Y.)* **52**, 403 (1969).

¹¹ E.P. Gross, *Nuovo Cimento* **20**, 454 (1961); L.P. Pitaevskii, *Zh. Eksp. Teor. Fiz.* **40**, 646 (1961) [*Sov. Phys. JETP* **13**, 451 (1961)].

¹² E. Krotscheck, Q.-X. Qian, and W. Kohn, *Phys. Rev. B* **31**, 4245 (1985).

¹³ E. Krotscheck and C.J. Tymczak, *Phys. Rev. B* **45**, 217 (1992).

¹⁴ B.E. Clements, J.L. Epstein, E. Krotscheck, and M. Saarela, *Phys. Rev. B* **48**, 7450 (1993).

¹⁵ S. Stringari and J. Treiner, *Phys. Rev. B* **36**, 8369 (1987).

¹⁶ S. Stringari and J. Treiner, *J. Chem. Phys.* **87**, 5021 (1987).

¹⁷ D. Vautherin and D.M. Brink, *Phys. Rev. C* **5**, 626 (1972).

¹⁸ C. Ji and M. Wortis, *Phys. Rev. B* **34**, 7704 (1986).

¹⁹ We note that this definition of $\chi(q)$ differs from the one of Ref. 1 by a factor ρ .

²⁰ R.A. Cowley and A.D.B. Woods, *Can. J. Phys.* **49**, 177 (1971); A.D.B Woods and R.A. Cowley, *Rep. Prog. Phys.* **36**, 1135 (1973).

²¹ S. Moroni, D.M. Ceperley, and G. Senatore, *Phys. Rev. Lett.* **69**, 1837 (1992); S. Moroni (private communication).

²² J. Boronat, J. Casulleras, and J. Navarro, *Phys. Rev. B* **50**, 3427 (1994).

²³ B.M. Abraham, Y. Eckstein, J.B. Ketterson, M. Kuchnir, and P.R. Roach, *Phys. Rev. A* **1**, 250 (1970).

²⁴ R. De Bruyn Ouboter and C.N. Yang, *Physica B* **44**, 127

- (1987).
- ²⁵ H.M. Guo, D.O. Edwards, R.E. Sarwinski, and J.T. Tough, *Phys. Rev. Lett.* **27**, 1259 (1971).
- ²⁶ M. Iino, M. Suzuki, and A.J. Ikushima, *J. Low Temp. Phys.* **61**, 155 (1985).
- ²⁷ L.B. Lurio *et al.*, *Phys. Rev. Lett.* **68**, 2628 (1992).
- ²⁸ T. Regge, *J. Low Temp. Phys.* **9**, 123 (1972).
- ²⁹ J.R. Henderson and Z.A. Sabeur, *J. Chem. Phys.* **97**, 6750 (1992); R. Evans, J.R. Henderson, D.C. Hoyle, A.O. Parry, and Z.A. Sabeur, *Mol. Phys.* **80**, 755 (1993); R. Evans, R.J.F. Leote de Carvalho, J.R. Henderson, and D.C. Hoyle, *J. Chem. Phys.* **100**, 591 (1994).
- ³⁰ M. Rasetti and T. Regge, in *Quantum Liquids*, edited by J. Ruvalds and T. Regge (North-Holland, Amsterdam, 1978), p. 227.
- ³¹ V.R. Pandharipande, J.G. Zabolitzky, S.C. Pieper, R.B. Wiringa, and U. Helbrecht, *Phys. Rev. Lett.* **50**, 1676 (1983); V.R. Pandharipande, S.C. Pieper, and R.B. Wiringa, *Phys. Rev. B* **34**, 4571 (1986).
- ³² P. Sindzingre, M.L. Klein, and D.M. Ceperley, *Phys. Rev. Lett.* **63**, 1601 (1989).
- ³³ M.V. Rama Krishna and K.B. Whaley, *Phys. Rev. Lett.* **64**, 1126 (1990); *J. Chem. Phys.* **93**, 746 (1990).
- ³⁴ S.A. Chin and E. Krotscheck, *Phys. Rev. B* **45**, 852 (1992).
- ³⁵ S.A. Chin and E. Krotscheck, *Phys. Rev. Lett.* **74**, 1143 (1995).
- ³⁶ R.N. Barnett and K.B. Whaley (private communication).
- ³⁷ J.P. Toennies, in *Chemical Physics of Atomic and Molecular Clusters*, Varenna, 1988, edited by G. Scoles (North-Holland, Amsterdam, 1990), p. 597.
- ³⁸ R. Melzer and J.G. Zabolitzky, *J. Phys. A* **17**, L565 (1984).
- ³⁹ G. Vidali, G. Ihm, H.Y. Kim, and M.W. Cole, *Surf. Sci. Rep.* **12**, 133 (1991).
- ⁴⁰ B.E. Clements, E. Krotscheck, and H.J. Lauter, *Phys. Rev. Lett.* **70**, 1287 (1993).
- ⁴¹ Marc Himbert, Ph.D. thesis, University Paris 6, 1987.
- ⁴² L. Pierre, H. Guignes, and C. Lhuillier, *J. Chem. Phys.* **82**, 496 (1985).
- ⁴³ C.G. Paine and G.M. Seidel, *Phys. Rev. B* **46**, 1043 (1992).
- ⁴⁴ P.A. Whitlock, G.V. Chester, and M.H. Kalos, *Phys. Rev. B* **38**, 2418 (1988).
- ⁴⁵ G. Zimmerli, G. Mistura, and M.H.W. Chan, *Phys. Rev. Lett.* **68**, 60 (1992).
- ⁴⁶ M. Casas and S. Stringari, *J. Chem. Phys.* **87**, 5021 (1990).
- ⁴⁷ M. Barranco and E.S. Hernandez, *Phys. Rev. B* **49**, 12078 (1994).
- ⁴⁸ R.P. Feynman, *Phys. Rev.* **94**, 262 (1954); E. Feenberg, *Theory of Quantum Fluids* (Academic Press, New York, 1969).
- ⁴⁹ K.A. Gernoth and M.L. Ristig, *Phys. Rev. B* **45**, 2969 (1992).
- ⁵⁰ R.J. Donnelly, J.A. Donnelly, and R.N. Hills, *J. Low Temp. Phys.* **44**, 471 (1981).
- ⁵¹ E.C. Svensson, V.F. Sears, A.D.B. Woods, and P. Martel, *Phys. Rev.* **21**, 3638 (1980).
- ⁵² W.G. Stirling, in *Excitations in Two-Dimensional and Three-Dimensional Quantum Fluids*, edited by A.F.G. Wyatt and H.J. Lauter, Vol. 257 of *NATO Advanced Study Institute, Series B: Physics* (Plenum, New York, 1991), p. 25.
- ⁵³ D. Pines, in *Excitations and Transport in Quantum Liquids*, edited by F. Bassani, F. Fumi, and M. P. Tosi, Proceedings of the International School of Physics "Enrico Fermi," Course LXXXIX, Varenna, 1983 (North-Holland, Amsterdam, 1985).
- ⁵⁴ B.E. Clements, H. Forbert, E. Krotscheck, and M. Saarela, *J. Low Temp. Phys.* **95**, 849 (1994).
- ⁵⁵ D.O. Edwards, J.R. Eckardt, and F.M. Gasparini, *Phys. Rev. A* **9** 2070 (1974); D.O. Edwards and W.F. Saam, in *Progress in Low Temperature Physics*, edited by D. F. Brewer (North-Holland, Amsterdam, 1978), Vol. II A, p. 283.
- ⁵⁶ H.J. Lauter, H. Godfrin, V.L.P. Frank, and P. Leiderer, in *Excitations in Two-Dimensional and Three-Dimensional Quantum Fluids* (Ref. 52), p. 419; H.J. Lauter, H. Godfrin, and P. Leiderer, *J. Low Temp. Phys.* **87**, 425 (1992).
- ⁵⁷ A. Latri, F. Dalfovo, L. Pitaevskii, and S. Stringari, *J. Low Temp. Phys.* **98**, 227 (1995).
- ⁵⁸ P.J. Shirron and J.M. Mochel, *Phys. Rev. Lett.* **67**, 1118 (1991).
- ⁵⁹ B.E. Clements, H. Forbert, E. Krotscheck, H.J. Lauter, M. Saarela, and C.J. Tymczak, *Phys. Rev. B* **50**, 6958 (1994).